Deterministic kinetic solvers for charged particle transport in semiconductor devices

M.J. Cáceres[1], J.A. Carrillo[2], I.M. Gamba[3], A. Majorana[4], and C.-W. Shu[5]

[1] Departamento de Matematica Aplicada, Universidad de Granada, 18071 Granada, Spain. caceresg@ugr.es
[2] ICREA (Institució Catalana de Recerca i Estudis Avançats) and Departament de Matemàtiques, Universitat Autònoma de Barcelona, E-08193 Bellaterra, Spain. E-mail: carrillo@mat.uab.es
[3] Department of Mathematics and ICES, The University of Texas at Austin, USA gamba@math.utexas.edu
[4] Dipartimento di Matematica e Informatica, Università di Catania, Catania, Italy majorana@dmi.unict.it
[5] Division of Applied Mathematics, Brown University, Providence, RI 02912, USA shu@dam.brown.edu

Summary. We review the main advances and developments in deterministic numerical methods for kinetic models in semiconductors. We describe the Boltzmann Transport Equation, as used in semiconductors community, with most of the standard inter- and intra-valley scattering operators for different materials. We discuss and compare several deterministic numerical methods proposed for its simulation. We also show how WENO methods perform in realistic 2D devices as double-gate MOSFETS. We compare their results to Multi-group-WENO methods in bulk material.

Keywords: Weighted Essentially Non-Oscillatory (WENO) schemes; Boltzmann Transport Equation (BTE); semiconductor device simulation; Metal Semiconductor Field Effect Transistor (MESFET); Metal Oxide Semiconductor Field Effect Transistor (MOSFET); Direct Simulation Monte Carlo (DSMC).

1 Introduction

Statistical models [F91, L00, MRS90, To93] are used to describe the electron transport in semiconductors at a mesoscopic level. The basic model is given by the Boltzmann Transport Equation (BTE) for semiconductors in the semiclassical approximation:

$$\frac{\partial f}{\partial t} + \frac{1}{\hbar}\nabla_{\mathbf{k}}\varepsilon \cdot \nabla_{\mathbf{x}} f - \frac{\mathfrak{e}}{\hbar}\mathbf{E} \cdot \nabla_{\mathbf{k}} f = Q(f), \tag{1}$$

where f represents the electron probability density function (**pdf**) in phase space $\mathbf{k}$ at the physical location $\mathbf{x}$ and time t. $\hbar$ and $\mathfrak{e}$ are physical constants; the Planck constant divided by 2π and the positive electric charge, respectively. The energy-band function ε is given by the Kane non-parabolic band model, which is a non-negative continuous function of the form

$$\varepsilon(\mathbf{k}) = \frac{1}{1+\sqrt{1+2\,\dfrac{\alpha}{m^*}\hbar^2\,|\mathbf{k}|^2}}\,\frac{\hbar^2}{m^*}\,|\mathbf{k}|^2\,, \tag{2}$$

where m^* is the effective mass and α is the non parabolicity factor. In this way we observe that setting $\alpha = 0$ in equation (2) the model is reduced to the widely used parabolic approximation.

The electric field $\mathbf{E}$ is self consistently computed by the Poisson equation:

$$\nabla_{\mathbf{x}}\left[\epsilon_r(\mathbf{x})\,\nabla_{\mathbf{x}}V\right] = \frac{\mathfrak{e}}{\epsilon_v}\left[\rho(t,\mathbf{x}) - N_D(\mathbf{x})\right], \tag{3}$$

$$\mathbf{E} = -\nabla_{\mathbf{x}}V, \tag{4}$$

since we take into account the electrostatics produced by the electrons and the dopants in the semiconductor. We represent the dielectric constant in a vacuum by ϵ_v and $\epsilon_r(\mathbf{x})$ labels the relative dielectric function depending on the material, $\rho(t,\mathbf{x}) = \int_{\Re^3} f(t,\mathbf{x},\mathbf{k})\,d\mathbf{k}$ is the electron density, $N_D(\mathbf{x})$ is the doping and V is the electric potential. Equations (1), (3)-(4) give the Boltzmann-Poisson system for electron transport in semiconductors.

The right-hand side of Equation (1) models the interaction of electrons with lattice vibrations of the crystal and can be written as

$$Q(f)(t,\mathbf{x},\mathbf{k}) = \int_{\mathbb{R}^3}\left[S(\mathbf{k}',\mathbf{k})f(t,\mathbf{x},\mathbf{k}') - S(\mathbf{k},\mathbf{k}')f(t,\mathbf{x},\mathbf{k})\right]\,d\mathbf{k}'\,, \tag{5}$$

where $S(\mathbf{k},\mathbf{k}')$ is the transition probability from state $\mathbf{k}$ to $\mathbf{k}'$ per unit of time for each scattering mechanism. Therefore, the collision term $Q(f)$ depends on the device semiconductor material. For Si-based technology, the scattering phenomena taken into account are: acoustic phonon and optical non-polar phonon, while for a GaAs device the scattering mechanisms are: impurities, acoustic phonon, non-polar optical phonon and polar optical phonon. Here, we will just give the expression of some of them relevant to discussions below. For instance, the transition probability for randomly placed impurities reads

$$S^{(imp)}(\mathbf{k},\mathbf{k}') = \frac{K_{imp}}{(|\mathbf{k}-\mathbf{k}'|^2+\beta^2)^2}\,\delta(\varepsilon'-\varepsilon),$$

with

$$K_{imp} = \frac{N_I Z^2 \mathfrak{e}^4}{4\pi^2\hbar\epsilon_v^2\epsilon_r^2}, \qquad \beta = \sqrt{\frac{\mathfrak{e}^2 N_I}{\epsilon_v\epsilon_r k_B T_L}},$$

where β is the inverse of the Debye length, N_I and $Z\,\mathfrak{e}$ are the impurities concentration and its charge, respectively, k_B is the Boltzmann constant and T_L is the lattice temperature. We refer to Table 1 for a complete list of the physical parameters.

The scattering with crystal vibrations in the acoustic mode is taken into account in the elastic approximation and is given by

$$S^{(ac)}(\mathbf{k},\mathbf{k}') = K_{ac}\,\delta(\varepsilon' - \varepsilon),$$

with

$$K_{ac} = \frac{k_B T_L \Xi_d^2}{4\pi^2 \hbar \rho_o v_s^2}.$$

Polar optical phonon scattering has a transition probability

$$S^{(p)}(\mathbf{k},\mathbf{k}') = K_p \frac{G(\mathbf{k},\mathbf{k}')}{|\mathbf{k}-\mathbf{k}'|^2}\left[n_p\delta(\varepsilon'-\varepsilon-\hbar\omega_p) + (1+n_p)\delta(\varepsilon'-\varepsilon+\hbar\omega_p)\right],$$

with

$$K_p = \frac{\hbar\omega_p \mathfrak{e}^2}{8\pi^2\hbar\epsilon_v}\left(\frac{1}{\epsilon_\infty} - \frac{1}{\epsilon_r}\right), \quad n_p = \frac{1}{\exp(\hbar\omega_p/(k_B T_L)) - 1},$$

$\hbar\omega_p$ the polar optical phonon energy, n_p its occupation number and the overlapping factor

$$G(\mathbf{k},\mathbf{k}') = \left[aa' + cc'\cos(\mathbf{k},\mathbf{k}')\right]^2,$$

with

$$a = \sqrt{\frac{1+\alpha\varepsilon}{1+2\,\alpha\varepsilon}}, \qquad a' = \sqrt{\frac{1+\alpha\varepsilon'}{1+2\,\alpha\varepsilon'}},$$

$$c = \sqrt{\frac{\alpha\varepsilon}{1+2\,\alpha\varepsilon}}, \qquad c' = \sqrt{\frac{\alpha\varepsilon'}{1+2\,\alpha\varepsilon'}}.$$

Before describe the last scattering, non-polar optical phonon, we recall the band structure of the GaAs material. On the lowest energy conduction band, the most important information comes from the absolute and local minima since they typically concentrate most of the electrons. These minima are called valleys and we will consider them as different populations in our model. In GaAs the most interesting part of the valley structure is given by an absolute minimum at the center of the Brillouin zone called the Γ-valley and four local minima through the crystal orientation called the L-valleys which are considered equivalent [To93]. In this way, the transport of electrons in each valley is studied by a linear Boltzmann Equation (1). Therefore, for a GaAs device the Boltzmann-Poisson system (1), (3)-(4) is augmented since we need to use two Boltzmann equations, one for each valley. Poisson equation couples both kinetic equations since the total density of electrons consists in an suitable average of the density of electrons in each valley. Moreover, electrons can jump

to different valleys, this fact is reflected in the collision term Q by means of the inter-valley scattering mechanism. Non-polar optical phonon scattering is considered in the inelastic approximation and both intra- and inter-valley and thus, we consider emission and absorption of phonons of energy $\hbar\omega_{np}$ (A, B denote different, or equal, valleys):

$$S^{(np)}(\mathbf{k}_A, \mathbf{k}_B) = K_{np}\left[n_{np}\delta(\varepsilon_B - \varepsilon_A - \hbar\omega_{np}^+) + (1+n_{np})\delta(\varepsilon_B - \varepsilon_A + \hbar\omega_{np}^-)\right],$$

with

$$K_{np} = \frac{(D_t K)^2}{8\pi^2\rho_0\omega_{np}}, \qquad n_{np} = \frac{1}{\exp(\hbar\omega_{np}/(k_B T_L)) - 1}$$

$$\hbar\omega_{np}^+ = \hbar\omega_{np} + \Delta_{AB}, \qquad \hbar\omega_{np}^- = \hbar\omega_{np} - \Delta_{AB}.$$

The occupation number n_{np} is given by the equilibrium Bose-Einstein distribution. GaAs solid-state properties imply that non polar optical phonon scattering contributes to the inter-valley scattering but only to the intra-valley scattering for the L-valley. $\Delta_{AB} = \varepsilon_{0A} - \varepsilon_{0B}$ is the energy gap between the minima of the two valleys.

In order to develop a competitive numerical scheme the equations are simplified by changing variables to suitable energy-type variables in which the scattering operators become either simple evaluations or linear integral operators with singular kernels. This change of variables was introduced first in [FO93] in the parabolic band approximation and in [MP01] for general dispersion relations for the energy formula (2). This change of variables and a suitable adimensionalization were performed for Si and GaAs devices [CGMS03-2, CCM06].

The main numerical tools to simulate the Boltzmann-Poisson system for semiconductor devices have practically been based on Direct Simulation Monte Carlo (DSMC) method. Since the dimension of the Boltzmann-Poisson system is 7, numerical simulations are heavily costly. To overcome this problem several approximated systems and corresponding deterministic numerical methods have been proposed in literature: spherical harmonics approximation, hydrodynamic models, diffusion limits leading to drift-diffusion equations, Child-Langmuir asymptotics, ... The literature of the different approximation systems is considerably large, therefore we just refer to [AH02, AMR03, BDMS01, CC95, D04, JS94, MRS90, Sel84] and the literature therein, not pretending at all to be exhaustive.

The earliest work in the direct deterministic simulation of Boltzmann-Poisson systems started with particle methods in [DDM90]. We should also mention the works of C. Ringhofer, see [R00, R03] and the references therein, where he has proposed a general approach by means of series expansion in momentum vector to solve the stationary and time dependent BTE. This strategy leads to a hyperbolic system for the coefficients of the expansion that depend both on time and position. Moreover, the proposed scheme can

deal with regimes close to drift-diffusion equations in a natural way. Recent developments have been done in [JPMRB06].

Starting in [CGJS00, CGS00], direct finite difference methods based on high-order WENO (weighted essentially non-oscillatory) approximations were used to compute the advection part of the transport equation for the 1-D relaxation-time kinetic system for semiconductors. In [CGS00] the considered model distinguishes the materials only with some representative parameters: mobility, mass and relaxation time. The collision operator (relaxation) does not take into account the different scattering mechanisms concerning the material of the device. However, the simplicity of this operator allows to validate the use of a WENO-scheme to simulate the spatial and velocity derivatives of the equation. Later, using the cited above change of variables [MP01] the real collision operators were analyzed, considering all possible scattering mechanisms in Si [CGMS02, CGMS03-2] and GaAs [CCM06], and thus even extended to 2D spatial semiconductors [CGMS03-3, CGMS06].

Recently, these developments have been coupled to alternative ideas producing other deterministic solvers which are applied to different semiconductor materials. A brief introduction to these schemes is given in Section 5. Here, we wish to cite the recent and relevant papers of a research group in Graz. In [AS05, AS05-2, DS04, DGS05, ES05, GS05, GM06, GS06] the numerical technique is used to solve the Boltzmann-Poisson system in 1D or 2D cases for semiconductor devices based on Si, or GaAs or AlGaN/GaN material. Moreover, they also consider [ASK04, GS04, GSb05] a model consisting of a couple of kinetic equations: one for the free electron and the other for the phonons, which are no longer constant. This model must be considered when hot phonon phenomena occur. The book by M. Galler [Ga05] furnishes both an introduction to semiconductor physics and a complete description of these numerical schemes; many examples of applications are also given.

We discuss in Section 2 the 1D case analyzing the results from the relaxation case to the full collision operator for GaAs devices. In Section 3, previous results are extended to dimension 2 where new difficulties arose to implement the boundary conditions. We conclude this section with simulations, as a example, for a double gate MOSFETs. Section 4 is devoted to summarize the works developed using alternative ideas in energy and angles variables by multi-group techniques borrowed from neutron transport numerical schemes. In Section 5, we will briefly state the goals achieved in this research and we will comment possible new directions in this field.

2 1D deterministic device simulations

WENO-schemes [JS96, Sh98] were used in [CGJS00, CGS00] to simulate the 1-D relaxation-time kinetic system for semiconductors. WENO approximations of the spatial and velocity derivatives were used coupled to explicit Runge-Kutta method for time evolution due to the stability of the WENO

approximation of the derivatives. This system is a first approximation of the Boltzmann-Poisson system for semiconductors; the right hand side of the equation is approximated by $\frac{1}{\tau}(M_{T_L}(v)\rho(f) - f)$, where the relaxation time τ is assumed constant and related to standard values of the mobility μ by $\mu = \frac{\mathfrak{e}}{m^*}\tau$ and M_{T_L} is the Maxwellian associated with this temperature

$$M_{T_L}(v) = \left(\frac{2\pi k_B T_L}{m^*}\right)^{-1/2} \exp\left(-\frac{m^* v^2}{2k_B T_L}\right).$$

Therefore, we observe that the particularities of the material are reflected only in the parameters τ and m^*. In [CGS00] the authors analyzed and compared their results with several classical approximations to the Boltzmann-Poisson system (hydrodynamics, drift-diffusion systems). The results were validated, also, with Monte Carlo (DSMC) results for silicon diodes in [ACGS01, CGMS03-1] and a numerical validation for the Child-Langmuir limit for semiconductors for Si and GaAs devices was shown in [CCD02].

Later, in [CGMS03-2] all the scattering mechanisms considered in a Si devices were taken into account. The complexity of the collision operator was overcome by considering the change of variables to suitable energy-type dimensionless variables. We write here the Boltzmann-Poisson system after the change of variables and the dimensionless process for the GaAs case [CCM06]. Since in this case two valleys have to be taken into account, we use the subindex A to call the different valleys: Γ and L, (for Si we can remove this index) and denote by $\bar{}$ the dimensionless variables and parameters. Equation (1) is written as:

$$\frac{\partial \Phi_A}{\partial t} + \frac{\partial}{\partial z}\left(a_1^A \Phi_A\right) + \frac{\partial}{\partial w_A}\left(a_2^A \Phi_A\right) + \frac{\partial}{\partial \mu_A}\left(a_3^A \Phi_A\right) = \bar{Q}(\Phi_A),\ A = \Gamma, L \quad (6)$$

where Φ_A is the new unknown function depending on dimensionless time $t \geq 0$, dimensionless spatial variable z, dimensionless energy w_A and cosine of the angle with respect to field direction μ_A. The flux coefficients are:

$$\begin{aligned} a_1^A &= a_1^A(w_A, \mu_A) = c_{1,A}\, \frac{\mu_A \sqrt{2\, w_A(1 + \bar{\alpha}_A w_A)}}{1 + 2\,\bar{\alpha}_A w_A}, \\ a_2^A &= a_2^A(w_A, \mu_A) = -c_{2,A}\, \bar{\mathbf{E}}\, \mu_A \frac{\sqrt{2\, w_A(1 + \bar{\alpha}_A w_A)}}{1 + 2\bar{\alpha}_A w_A}, \\ a_3^A &= a_3^A(w_A, \mu_A) = -c_{2,A}\, \bar{\mathbf{E}}\, \frac{1 - \mu_A^2}{\sqrt{2\, w_A(1 + \bar{\alpha}_A w_A)}}, \end{aligned} \quad (7)$$

where

$$c_{1,A} = \frac{t_*}{l_*}\sqrt{\frac{k_B T_L}{m_A^*}} \quad \text{and} \quad c_{2,A} = \sqrt{\frac{m_X^*}{m_A^*}}, \quad (8)$$

where t_*, l_* and m_X^* are the characteristic time, length and mass respectively. The Poisson equation (3) is written as:

$$\begin{aligned}\Delta_z \bar{V}(t,z) = c_p \Bigg(& c_\Gamma \int_0^\infty \int_{-1}^1 \Phi_\Gamma(t,z,w_\Gamma,\mu_\Gamma)\, d\mu_\Gamma\, dw_\Gamma \\ & + c_L \int_0^\infty \int_{-1}^1 \Phi_L(t,z,w_L,\mu_L)\, d\mu_L\, dw_L - \bar{N}_D(z) \Bigg)\end{aligned} \tag{9}$$

with c_p, c_Γ and c_L defined as

$$c_p = \frac{\mathfrak{e}^2\, t_*\, l_*\, m_X^*\, k_B T_L}{\epsilon_v \epsilon_r\, \hbar^3},\ c_\Gamma = 2\,\pi\, Z_{L\Gamma} \left(\frac{m_\Gamma^*}{m_X^*}\right)^{3/2},\ c_L = 2\,\pi\, Z_{\Gamma L} \left(\frac{m_L^*}{m_X^*}\right)^{3/2}, \tag{10}$$

where $Z_{\Gamma L}$ and $Z_{L\Gamma}$ are the degeneration numbers from Γ-valley to L-valley and vice versa. Returning to (6), we show the dimensionless collision term $\bar{Q}$:

$$\begin{aligned}\bar{Q}(\Phi_A) = s_A(w_A) \int_{-1}^1 \Big\{ & 2\,\pi\, c_{3,A} \Phi_A(w_A,\mu'_A) + c_{4,A} I_{4,A}(w_A,\mu_A,\mu'_A) \Phi_A(w_A,\mu'_A) \\ & + c_{5,A} \Big[I^+_{5,A}(w_A, w_A - \alpha_p, \mu_A, \mu'_A) \Phi^+_A(w_A - \alpha_p, \mu'_A) \\ & + a_p I_{5,A}(w_A, w_A + \alpha_p, \mu_A, \mu'_A) \Phi_A(w_A + \alpha_p, \mu'_A) \Big] \\ & + c_{6,A}\, 2\,\pi \left[\Phi^+_A(w_A - \alpha_{np}, \mu'_A) + a_{np}\, \Phi_A(w_A + \alpha_{np}, \mu'_A) \right] \Big\}\ d\mu'_A \\ & - \Bigg\{ 4\,\pi\, c_{3,A} s_A(w_A) + 4\,\pi\, c_{4,A} \frac{s_A(w_A)}{{\beta_A}^2 (4\, q_A(w_A) + {\beta_A}^2)} \\ & + c_{5,A} \Big[N_{5,A}(w_A, w_A + \alpha_p) s_A(w_A + \alpha_p) \\ & + a_p\, N^+_{5,A}(w_A, w_A - \alpha_p) s^+_A(w_A - \alpha_p) \Big] \\ & + c_{6,A}\, 4\pi\ \left[s_A(w_A + \alpha_{np}) + a_{np}\, s^+_A(w_A - \alpha_{np}) \right] \Bigg\} \Phi_A(w_A,\mu_A) \\ & + Z_{AB} s_A(w_A)\, c_{7,B}\, 2\pi \int_{-1}^1 \left[\Phi^+_B(w_A - \alpha_{np} - \bar{\Delta}_{BA}, \mu_B) \right. \\ & \left. + a_{np} \Phi^+_B(w_A + \alpha_{np} - \bar{\Delta}_{BA}, \mu_B) \right]\ d\mu_B \\ & - Z_{AB}\, c_{7,B}\, 4\pi \left[s^+_B(w_A + \alpha_{np} + \bar{\Delta}_{AB}) \right. \\ & \left. + a_{np}\, s^+_B(w_A - \alpha_{np} + \bar{\Delta}_{AB}) \right] \Phi_A(w_A,\mu_A),\end{aligned} \tag{11}$$

where $s_A(w_A)$ is the Jacobian of the coordinate transformation up to constants (the notation $^+$ means the positive part of the function), $I_{4,A}$, $I_{5,A}$,

$N_{5,A}$ are functions which depend on the integral parts of the collision operator, $q_A(w) = 2w_A(1 + \bar{\alpha}_A w_A)$, and $c_{3,A}$,$c_{4,A}$, $c_{5,A}$,$c_{6,A}$ and $c_{7,A}$ are constants related to the different scatterings. The complexity of this term resides in the new, compared to Si, scattering mechanisms: impurity, optical polar phonon and optical non-polar phonon for intervalleys. For a Silicon device the collision operator is approximated by simple evaluations in mesh points. In GaAs the collision operator is more complicated since it involves the functions I_4 and I_5, coming from impurities and optical phonon scattering respectively, which present integrable singularities. This complexity of the collision operator produces a new numerical difficulty which is solved in [CCM06] by a suitable numerical approximation of the gain term.

The numerical scheme used is a conservative finite difference WENO scheme of fifth order in the transport variables and the evolution on time is done by a third order TVD Runge-Kutta method. For details we refer to [CGMS03-2] where the numerical scheme is explained. Boundary conditions are basically zero flux on the boundaries in energy and angle and inflow maxwellian boundary conditions in space, see Section 3 for boundary conditions for 2D case. The Poisson equation is discretized and numerically solved by a standard central finite difference scheme. Stability in time for the resulting scheme is ensured by computing time steps verifying a CFL condition. The CFL condition may become severe whenever high field regions appear in the device, investigations to avoid this problem are under way.

The main difference, from the numerical point of view, between Si and GaAs is the complexity of the last one, since two valleys have to be considered. This fact produces numerical difficulties for the preservation of total charge due to the inter-valley scattering mechanisms in the homogeneous case and the singular character of the kernels of the impurities and polar optical phonon scattering. The presence of two Boltzmann equations for the GaAs case produces a larger computational cost that can be overcome by a parallelized implementation [MCM05], in which the authors compute for the first time I-V curves for 2D devices by deterministic schemes.

In [CGMS03-2] the numerical scheme is tested for two $n^+ - n - n^+$ diodes of total length of 1 μm and 0.25 μm, with 400 nm and 50 nm channels located in the middle of the device, respectively. Deterministic results are compared with DSMC and with other classical approximations of the Boltzmann-Poisson system: drift-diffusion, hydrodynamic and kinetic relaxation models discussing how good the approximation of the real collision operator by a relaxation model [CGS00] is. Different phonon frequencies are taken into account in [MMM04] performing comparisons to DSMC commercial solvers.

In [CCM06] the WENO-solver proposed is validated by computing the electron valley occupancy, velocity and energy of the homogeneous case, bulk material, and by comparing with the DSMC results. They show the well-known experimental phenomena of the material [To93]. It was the first step in order to analyze the transport of electrons in $n^+ - n_i - n^+$ diodes and Gunn-oscillators [CJSW98, MR05]. Here, n_i is the intrinsic concentration of

the material and the GaAs diode had a channel length of 0.25 μm for a total length of 0.55 μm.

As a summary of both works [CGMS03-2, CCM06], we can point out that the main contribution has been the derivation of a fully deterministic solver for the BTE for semiconductors including all the relevant scattering mechanisms of the considered material. This solver allows us to compute the noise-free evolution on time of the distribution function at every point of the device and consequently all the moments of the distribution function, i.e., hydrodynamical quantities and the stabilization in time towards the steady state.

As an example of these simulations, we emphasize here that the steady state in some points of the channel of the device is far from being shifted Maxwellian distribution showing purely kinetic characteristics. Fig. 1 shows the distribution function in Cartesian coordinates for valleys Γ and L with 0.75 V applied bias at room temperature 300 K at point $z = 0.399667\,\mu m$ after $t = 3\,ps$. Comparing Si results to GaAs results, the asymmetry in the distribution function is more relevant in GaAs for the Γ-valley distribution than in Si. Discrete points of the simulations were simply joined by lines.

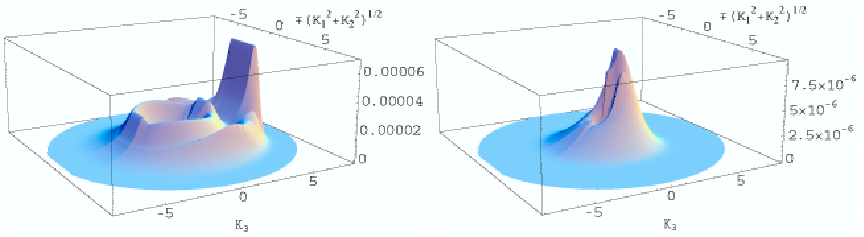

Fig. 1. GaAs device. Left: Γ-valley distribution. Right: L-valley distribution. Both in Cartesian coordinates at point $z = 0.399667\,\mu m$ at time $t = 3\,ps$ with 0.75 V applied bias at room temperature 300 K.

This scheme has been adapted to bipolar p-n junctions [GCG1, GCG2]. Here, we deal again with a system of two kinetic equations for holes and electrons coupled through the Poisson equation but also we have new terms due to recombination and generation of electron-hole pairs.

Let us finally mention that improvements in the WENO methods in order to reduce its computational cost have been explored by improving the time discretization [AS05], by adapting better the energy discretization [ARS05] and by imposing different uniform discretizations in different parts of the domain [GCG2, AS05-2].

3 2D deterministic device simulations

The change of variables and the dimensionless process used in 1D can be extended to the 2D case. The Boltzmann equation (see [CGMS03-3]) is written, in terms of the new unknown Φ, as

$$\frac{\partial \Phi}{\partial t} + \frac{\partial}{\partial x}(a_1 \Phi) + \frac{\partial}{\partial y}(a_2 \Phi) + \frac{\partial}{\partial \omega}(a_3 \Phi) + \frac{\partial}{\partial \mu}(a_4 \Phi) + \frac{\partial}{\partial \phi}(a_5 \Phi) = \bar{Q}(\Phi), \quad (12)$$

where the flux functions a_i are given by

$$\begin{aligned}
a_1(\omega) =& \frac{1}{t_*} \frac{\mu s(\omega)}{(1+2\alpha_\kappa \omega)^2} \\
a_2(\omega, \mu, \phi) =& \frac{1}{t_*} \frac{\sqrt{1-\mu^2} s(\omega) \cos\phi}{(1+2\alpha_\kappa \omega)^2} \\
a_3(t,x,y,\omega,\mu,\phi) =& -\frac{1}{t_*} \frac{2 s(\omega)}{(1+2\alpha_\kappa \omega)^2} \left[E_x(t,x,y)\mu \right. \\
& \left. + E_y(t,x,y)\sqrt{1-\mu^2}\cos\phi \right] \\
a_4(t,x,y,\omega,\mu,\phi) =& -\frac{1}{t_*} \frac{1+2\alpha_\kappa \omega}{s(\omega)} \sqrt{1-\mu^2} \left[E_x(t,x,y)\sqrt{1-\mu^2} \right. \\
& \left. - E_y(t,x,y)\mu\cos\phi \right] \\
a_5(t,x,y,\omega,\mu,\phi) =& \frac{E_y(t,x,y)}{t_*} \frac{\sin\phi}{\sqrt{1-\mu^2}} \frac{1+2\alpha_\kappa \omega}{s(\omega)},
\end{aligned}$$

Here, t appears with dimensions in contrast to previous section, from which the factor t_* appears in the flux coefficients. We remove the subindex A since we consider the Si case for simplicity. For GaAs, the differences, as in 1D case, are the presence of other scattering mechanisms and two relevant valleys, consequently two Boltzmann equations have to be considered. Therefore, 2D case for GaAs can also be done without further problems. In 2D case the unknown Φ depends on t (time), x, y (space variables), w (dimensionless energy), μ (cosine of the angle with respect to the x-axis) and ϕ (azimuthal angle).

Results of 2D case were presented in [CGMS03-3] for MESFET devices and in [MCM05] considering a parallelization of the numerical code. This deterministic solver was improved in [CGMS06] clarifying the implementation of the boundary conditions and the nature of boundary singularities in the electric field. The improved scheme was tested with a stochastic DSMC solver. We summarize here both issues, see [CGMS06] for details.

3.1 Boundary conditions

We consider semiconductor devices whose boundaries can be separated in four kinds of regions: gates, contact areas, insulated areas and contact boundary

between the semiconducting and the oxide regions (the last one for the MOSFET case only).

The boundary conditions associated to the electrostatic potential, (i.e. solutions of the Poisson equation (3)-(4)) are: prescribed potential (Dirichlet type conditions) at the source, drain, and gate contacts, and insulating (homogeneous Neumann conditions) on the remainder of the boundary.

The boundary conditions imposed to the numerical probability density function (**pdf**) approximating the solution of the BTE are as follows:

Source and drain contacts: numerical boundary conditions must approximate neutral charges. Here we employ a buffer layer of ghost points outside both the device contact source and drain areas and use conditions (2.1) from [CGMS06].

Under the assumption that highly doped regions $n^+(x, y)$ are slowly varying (i.e. of very small total variation norm), the corresponding small Debye length asymptotics yield neutral charges away from the endpoints of the contact boundary regions. Consequently, the total density ρ (zero order moment) and its variation takes asymptotically, in Debye length, the values of $n^+(x, y)$ away from the contact endpoints. This is the well-known limit for drift-diffusion systems [MRS90], and we observe that this is also the case for the kinetic problem, provided the kinetic solution satisfies approximately neutral charge conditions at these contact boundaries.

Gate contacts: the numerical boundary condition yields an estimated incoming mean velocity which represents a transversal electric field effect due to the gate contacts. These conditions, given in (2.3) from [CGMS06], or (2.4) for its integrated form, are of Robin (or mixed) type, which are the natural conditions for a simulation of a gate contact in an oxide region. This form of boundary conditions follows from classical asymptotics corresponding to *thin shell* elliptic and parabolic type problems with Dirichlet data in the *thin outer shell* domain and a core larger-scale domain, where classical transmission conditions link the force fields corresponding to both domains which combine into a Robin (mixed-type condition (2.8) from [CGMS06]). The two dimensional asymptotic boundary condition for the Poisson system linking the oxide and semiconductor region yielding a Robin type condition was rigorously studied in [Ga93-1, Ga93-2]

Insulating walls or contact boundary between the semiconducting and the oxide regions: In both of these cases we impose classical elastic specular boundary reflection conditions for numerical probability density function as in (2.10) from [CGMS06].

3.2 Appearance of singularities

It is well-known that solutions of the Poisson equation develop singularities in a bounded domain, with a Lipschitz boundary and a boundary condition that changes type from Dirichlet to homogeneous Neumann or Robin type data

on both sides of a conical wedge, with an angle $0 \leq \vartheta \leq 2\pi$, whose vertex is at the point of data discontinuity. The solution will develop a singularity at the vertex point depending on the angle ϑ. Indeed, for an elliptic problem in a domain with data-type change, the solution remains bounded with a radial behavior of a power less than one if $\pi/2 \leq \vartheta \leq 2\pi$. Its gradient then becomes singular (see for instance Grisvard [Gr85] for a survey on boundary value problems of elliptic PDE's in a non-convex domain, and Gamba [Ga90], [Ga93-1] for a rigorous study of a drift-diffusion Poisson system in a MOSFET type geometry). Therefore, in particular, the electric potential presents singularities and consequently singularities appear, also, in the electric field. Regardless, the deterministic solver presented is high order accurate. Consequently, elliptic and parabolic descriptions of the density flow at the drift-diffusion level remain with the same singular boundary behavior, even though mobilities functions are saturated quantities; that is, they are bounded functions of the magnitude of the electric field [Ga93-2]. In fact, these conditions have been used for two dimensional drift-diffusion simulations of MESFET devices and this singular boundary behavior was obtained [CC95].

We stress that our calculations resolve this singular boundary behavior as shown in Fig. 4 at the boundary points corresponding to the junction of the doping profile abrupt changing in variation to the oxide regions and gate contacts.

In view of this boundary asymptotic behavior at the macroscopic level and the numerical results we obtain for the deterministic solutions of the BTE-Poisson system and its moments, we conjecture in [CGMS06] that the moments of the particle distribution function $f(t, \mathbf{x}, \mathbf{k})$ have *the same spatial asymptotic behavior as the density solution of the drift-diffusion problem* at the boundary points with a discontinuity in the data. In other words, the collision mechanism preserves the spatial regularity of the **pdf** as though its zeroth moment would satisfy the drift-diffusion equations, even though the numerical evidence indicates that the average of the **pdf** (i.e. density) will not evolve according to such a simple macroscopic model.

3.3 2D Simulation Example: Double gate MOSFETs

The WENO-BTE solver is, again, a fifth order finite difference WENO scheme coupled with a third order TVD Runge-Kutta time discretization to solve (12) as that used in [CGMS06].

The Poisson equation (3) for the potential V and the electric field (4) are solved by the standard central difference scheme, with the given V_{bias} boundary conditions at the source, drain and gate.

A realistic device used by electronic engineers for which the scheme presented above can be applied is double-gate (DG) MOSFET. We show simulations for a DG-MOSFET where its structure is described in Fig. 2: two bands of oxide of thickness $2\,nm$ sandwich a band of Si of $24\,nm$ where electrons

transit. Two gates (top and bottom) with $50\,nm$ of length are considered at $50\,nm$ of the source.

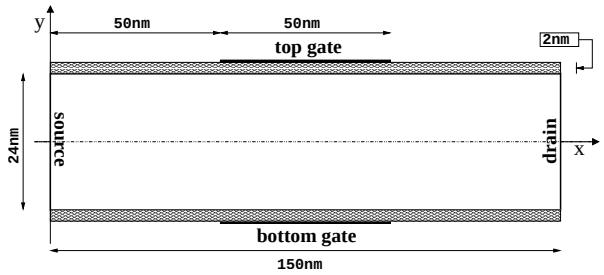

Fig. 2. Schematic representation of a double gate MOSFET

The voltage gate is $1.06\,V$ for both, while the drain applied bias is $1.6\,V$. A "V"-shaped doping profile as in [BSF03] was taken into account: doping concentration in the center of the channel is $10^{15}\,cm^{-3}$, while in the edges of the channel is $5 \times 10^{18}\,cm^{-3}$, see Fig. 3. The acceptors concentration is $10^{10}\,cm^{-3}$.

Boundary conditions were described in Section 3.1. Due to the symmetry of the device in the y-component, the device can be simulated for $y > 0$ only and the results for the other part of the device can be obtained by symmetry. Electron transport only happens in the semiconductor Si part of the device, therefore the BTE is only solved in this area, while Poisson equation is solved in the whole device to take into account the presence of the gates.

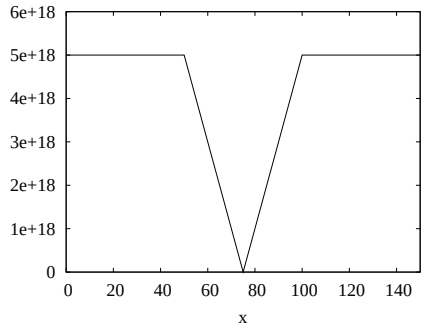

Fig. 3. Doping profile of the double gate MOSFET

As usual the BTE is simulated until the hydrodynamical quantities stabilize on time. In this sense, we consider that numerically the steady state has been achieved. In Fig. 4 we show the density, potential and energy of this stationary state. We observe two regions of the device with a high concentration

of electrons close to the gates. Electron are accelerated by the gate voltages and thus, the energy achieves its maximum value around the end of the gates, at $100\,nm$ of the source.

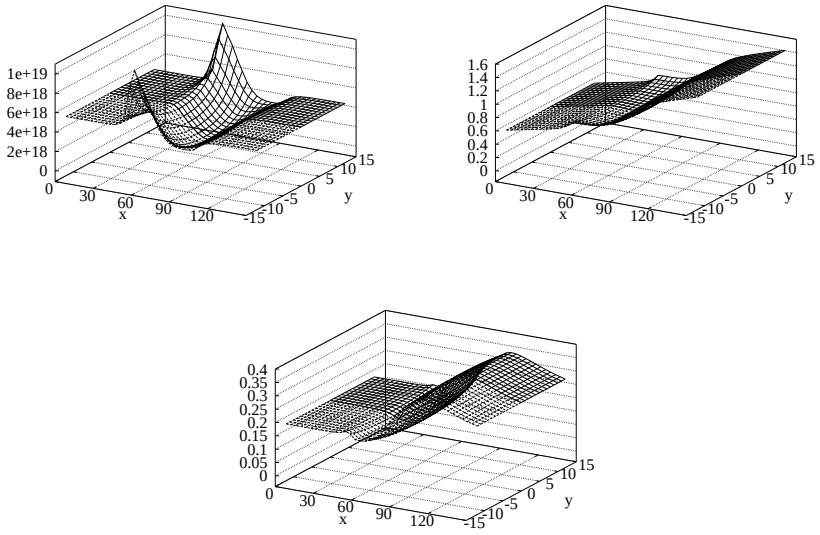

Fig. 4. Double-gate MOSFET device. Top left: the charge density ρ (cm^{-3}); top right: the electric potential V; bottom: the energy $\mathcal{E}$ (eV). Units in x and y are nm

4 The Multigroup-WENO Model Equations

This numerical technique consists of imposing an ansatz for the solution in the momentum variables: energy and angles, while keeping the dependence on time and position through the expansion coefficients. Ideas of multi-group techniques are not far from the general series expansion methods analyzed in [R00]. In a first step, assuming that the distribution function depends only on $\mathbf{k}$ through the coordinates $w \in [0, w_{max}]$, $\mu \in [-1, 1]$, we discretize them via

$$\begin{aligned} w_{i+1/2} &= i\Delta w, & i &= 0, 1, \ldots, N, & \Delta w &= w_{max}/N, \\ \mu_{j+1/2} &= -1 + j\Delta\mu, & j &= 0, 1, \ldots, M, & \Delta\mu &= 2/M, \end{aligned}$$

with two suitably chosen integers N and M. Here, w_{max} is a maximum value for the dimensionless energy, related to the physically studied process, for which we have to check that $\Phi(t, \mathbf{x}, w_{max}, \mu)$ is negligible for all t, $\mathbf{x}$ and μ.

In the case of a unique valley, the unknown function Φ is approximated by the finite sum

$$\Phi(t,\mathbf{x},w,\mu) \approx \sum_{i=1}^{N}\sum_{j=1}^{M} n_{ij}(t,\mathbf{x})\lambda_{w_i}(w)\,\lambda_{\mu_j}(\mu) \tag{13}$$

containing $N \times M$ coefficients $n_{ij}(t,\mathbf{x})$ and where the functions $\lambda_{w_i}(w)$ and $\lambda_{\mu_j}(\mu)$ can be chosen in different ways. The first possibility is to assume that $\lambda_{w_i}(w) = \delta(w_i - w)$ and $\lambda_{\mu_j}(\mu) = \delta(\mu_j - \mu)$, where δ is the Dirac distribution. Alternatively, they can be defined by

$$\lambda_{w_i}(w) = \begin{cases} \dfrac{1}{\Delta w}, & \text{if } w \in [w_{i-1/2}, w_{i+1/2}], \\ 0, & \text{otherwise,} \end{cases} \tag{14}$$

and the other function analogously. Recently, a modified approximation for the distribution function is proposed, introducing a weight function $p(w)$, such that

$$\Phi(t,\mathbf{x},w,\mu) \approx p(w)\sum_{i=1}^{N}\sum_{j=1}^{M} n_{ij}(t,\mathbf{x})\lambda_{w_i}(w)\,\lambda_{\mu_j}(\mu)\,, \tag{15}$$

where the function λ can be defined as above. The main advantage of introducing the function p is in taking into account the singularities or the shape of Φ. In [GM06], $p(w) = s(w)$ was assumed; so, apart from a constant factor Φ/s is the original distribution function f and the singularity at $w = 0$ is removed. The evolution equations for the coefficients n_{ij} are constructed as suggested by the method of weighted residuals. The ansatz (13) or (15) is inserted into the dimensionless Boltzmann equation and the result is integrated over the cells

$$\mathcal{Z}_{ij} = [w_{i-1/2}, w_{i+1/2}] \times [\mu_{j-1/2}, \mu_{j+1/2}].$$

This procedure yields a set of $N \times M$ partial differential equations for the n_{ij}. Therefore, WENO routines are used to obtain accurate numerical solutions. The flux through the cells $\mathcal{Z}_{ij}$, corresponding to the integration of the terms of the free streaming operator containing the partial derivatives with respect to the variables w and μ, is treated by using a simple formula based on the Min-Mod slope limiter. Details of the full general procedure are given in [Ga05, GM06].

This approach for solving the transport equation has some advantages and disadvantages with respect to the full WENO scheme. The multigroup-WENO technique (MW) is simple to use also in the case of not uniform grid in the (w,μ) space and the function $p(w)$ may be related to physical expectations (for instance, shape or tail of Φ). Moreover, it is requires less CPU time, due to the easy treatment of the force term in the Boltzmann equation. The main disadvantage is the loss of the accuracy in the approximation of the force term. Although the order of error is comparable with those coming from the

approximation of the collision operator, the presence of strong electric field enlarges the numerical error. This can be meaningful, as the moments of the distribution functions are evaluated. In order to show this, we have solved

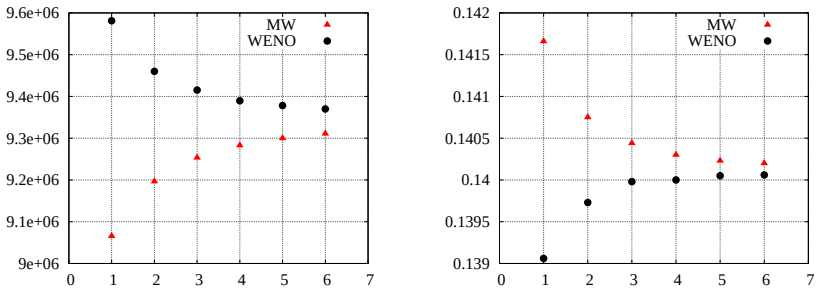

Fig. 5. Left: The velocity in cm/s. Right: The energy in eV.

the simple typical problem of the homogeneous charge transport in a bulk silicon device having a constant doping profile and a constant applied electric field. We use the full WENO scheme and the multigroup model based on Equation (15). The main thermodynamical quantities are the velocity and the energy. In left Fig. 5 we show the electron mean velocity for different grid sizes. The index i of x-axis corresponds to the values of the integer N and M (w_{max} is not changed) according to the following rule

$$N = 20 + i \times 20 \quad M = 8 + i \times 4 \quad (i = 1, 2, ..., 6)\,.$$

Right Fig. 5 shows mean energy results. The value of the electric field is 30 KV/cm.

It is evident the better accuracy of the WENO scheme than the MW method. So, if we require high accurate solutions, then WENO approach is preferable, since it needs fewer grid points than the other. We do not have the saving of CPU time of the multigroup technique, because we must increase the number of grid points. When we use a coarse grid, both results are reasonable. In this test we have used a moderate electric field; if we increase its value, then the differences are more emphasized.

5 Conclusions and future developments

The works developed during the last 5 years devoted to WENO methods conclude that they lead to high-order accurate solutions of the BTE for different materials and geometries. They actually represent benchmarks for hydrodynamic or drift-diffusion solvers that can be tested against them fairly. However, they present a significant computational cost that can be reduced

by computer techniques: parallelization and dynamic memory, or by tuning different numerical aspects: time discretization, energy discretization, multi-level/multi-grid methods, multi-resolution approaches, ... Some of them have already been recently tackled. We think multi-resolution approaches could lead to a tremendous reduction in computational time and multi-grid methods will ease the restriction to uniform grids. Summarizing WENO-based methods present two main disadvantages: a large computational cost mainly due to the CFL condition and the need of working with uniform (or smooth) spatial grids.

The search of new deterministic numerical methods for the BTE should continue keeping in mind the mentioned limitations of WENO-based methods. Methods allowing to take larger advection steps avoiding CFL conditions while keeping good accuracy will be surely a good alternative to WENO methods. Semilagrangian methods coupled to splitting techniques used for a long time in the simulation of Vlasov-type systems in plasma physics could be a good alternative [CV06].

On the other hand, to use non-structured grids is important in 2D real device simulation since the transport of electrons usually happens in narrow areas inside the device. Local discontinuous Galerkin methods are an alternate numerical technique in this direction. Recent developments in numerical and analytical studies for these type of solvers and simulations have been performed in [GP06].

Acknowledgments

Research of the first two authors is supported by DGI-MEC (Spain) project MTM2005-08024. Research of the third author is supported by NSF grant DMS-0204568. Research of the fourth author is supported by the Italian COFIN 2004. Research of the last author is supported by ARO grant W911NF-04-1-0291 and NSF grant DMS-0510345. We thank the Institute of Computational Engineering and Sciences (ICES) at the University of Texas for partially supporting this research. We thank José A. Cañizo for editing Fig. 1.

References

[ACGS01] Anile, A.M.; Carrillo, J.A.; Gamba, I.M.; Shu, C.-W.: Approximation of the BTE by a relaxation-time operator: simulations for a 50nm-channel Si diode, VLSI Design, **13**, (2001), 349-354.

[AH02] Anile, A.M.; Hern, S.D.: Two-population hydrodynamical models for carrier transport in gallium arsenide: simulation of gunn oscillations, VLSI Design, **15**, 681–693 (2002).

[AMR03] Anile, A.M.; Mascali, G.; Romano, V.: Recent developments in hydrodynamical modeling of semiconductors, Mathematical problems in semiconductor physics, Lecture Notes in Math., **1823**, 1–56 (2003).

[ASK04] Auer, C.; Schürrer, F.; Koller, W.: A semicontinuous formulation of the Bloch-Boltzmann-Peierls equations, SIAM J. Appl. Math., **64**, (2004), 1457–1475.

[AS05] Auer, C.; Schürrer, F.: Efficient time integration of the Boltzmann-Poisson system applied to semiconductor device simulation, to appear in J. Comput. Electron.

[AS05-2] Auer, C.; Majorana, A.; Schürrer, F.: Numerical schemes for solving the non-stationary Boltzmann-Poisson system for two-dimensional semiconductor devices, ESAIM: Proceedings, **15**, (2005), 75–86.

[ARS05] Auer, C.; Russo, G.; Schürrer, F.: Adaptive energy discretization of the semiconductor Boltzmann equation, preprint.

[BDMS01] Ben Abdallah, N.; Degond, P.; Markowich, P.; Schmeiser, C.: High field approximations of the spherical harmonics expansion model for semiconductors, Z. Angew. Math. Phys., **52**, (2001), 201–230.

[BSF03] Bufler, F.M.; Schenk, A.; Fichtner, W.: Monte Carlo hydrodynamic and drift-diffusions simulation of scaled double-gate MOSFETs, J. Comput. Electron., **2**, (2003), 81–84.

[CCD02] Cáceres, M.J.; Carrillo, J.A.; Degond, P.: The Child-Langmuir limit for semiconductors: a numerical validation, ESAIM: Mathematical Modelling and Numerical Analysis, **36**, (2002), 1161–1176.

[CCM06] Cáceres, M.J.; Carrillo, J.A.; Majorana, A.: Deterministic simulation of the Boltzmann-Poisson system in GaAs-based semiconductors, SIAM Journal of Scientific Computing, **27**, (2006), 1981–2009.

[CGS00] Carrillo, J.A.; Gamba, I.M.; Shu, C.-W.: Computational macroscopic approximations to the 1-D relaxation-time kinetic system for semiconductors, Physica D, **146**, (2000), 289–306.

[CGMS03-1] Carrillo, J.A.; Gamba, I.M.; Muscato, O.; Shu, C.-W.: Comparison of Monte Carlo and deterministic simulations of a silicon diode, IMA Volume Series **135**, (2003), 75–84.

[CGMS02] Carrillo, J.A.; Gamba, I.M.; Majorana, A.; Shu, C.-W.: A WENO-solver for the 1D non-stationary Boltzmann–Poisson system for semiconductor devices, J. Comput. Electron., **1**, (2002), 365–370.

[CGMS03-2] Carrillo, J.A.; Gamba, I.M.; Majorana, A.; Shu, C.-W.: A WENO-solver for the transients of Boltzmann–Poisson system for semiconductor devices. Performance and comparisons with Monte Carlo methods, J. Comput. Phys., **184**, (2003), 498–525.

[CGMS03-3] Carrillo, J.A.; Gamba, I.M.; Majorana, A.; Shu, C.-W.: A direct solver for 2D non-stationary Boltzmann-Poisson systems for semiconductor devices: a MESFET simulation by WENO-Boltzmann schemes, J. Comput. Electron., **2**, (2003), 375–380.

[CGMS06] Carrillo, J.A.; Gamba, I.M.; Majorana, A.; Shu, C.-W.: 2D semiconductor device simulations by WENO-Boltzmann schemes: efficiency, boundary conditions and comparison to Monte Carlo methods, J. Comput. Phys., **214**, (2006), 55–80.

[CV06] Carrillo, J.A.; Vecil, F.: Non oscillatory interpolation methods applied to Vlasov-based models, preprint.

[CGJS00] Cercignani, C.; Jerome, J.W.; Gamba, I.M.; Shu, C.-W.: Device Benchmark Comparisons via Kinetic, Hydrodynamic, and High-Field Models, Computer Methods in Applied Mechanics and Engineering, **181**, (2000), 381–392.

[CC95] Chen, Z.; Cockburn, B.: Analysis of a finite element method for the drift-diffusion semiconductor device equations: the multidimensional case, Num. Math., **71**, (1995), 1–28.

[CJSW98] Chen, G.-Q.; Jerome, J.W.; Shu, C.-W.; Wang, D.: Two carrier semiconductor device models with geometric structure and symmetry properties, Modelling and Computation for Applications in Mathematics, Science, and Engineer ing (ed. J. Jerome), Oxford University Press, 103–140, (1998).

[DDM90] Degond, P.; Delaurens, F.; Mustieles, F.J.: Semiconductor modelling via the Boltzmann equation, Computing Methods in Applied Sciences and Engineering, SIAM, 311-324 (1990).

[D04] Degond, P.: Macroscopic limits of the Boltzmann equation: a review, Modeling and computational methods for kinetic equations, Model. Simul. Sci. Eng. Technol., Birkhäuser Boston, 3–57 (2004).

[DS04] Domaingo, A.; Schürrer, F.: Simulation of Schottky barrier diodes with a direct solver for the Boltzmann-Poisson system, J. Comput. Electron., **3**, (2004), 221–225.

[DGS05] Domaingo, A.; Galler, M.; Schürrer, F.: A combined multicell-WENO solver for the Boltzmann-Poisson system of 1D semiconductor devices, Compel, **24**, (2005), 1311–1327.

[ES05] Ertler, C.; Schürrer, F.: A deterministic study of hot phonon effects in a 2D electron gas channel formed at an AlGaN/GaN heterointerface, to appear in J. Comput. Electron.

[FO93] Fatemi, E.; Odeh, F.: Upwind finite difference solution of Boltzmann equation applied to electron transport in semiconductor devices, J. Comput. Phys., **108**, (1993), 209–217.

[F91] Ferry, D.K.: Semiconductors, Maxwell MacMillian: New-York, 1991.

[GS04] Galler, M.; Schürrer, F.: A deterministic solution method for the coupled system of transport equations for the electrons and phonons in polar semiconductors, J. Phys. A, **37**, (2004), 1479–1497.

[GS05] Galler, M.; Schürrer, F.: A deterministic solver for the 1D non-stationary Boltzmann-Poisson system for GaAs devices: bulk GaAs and GaAs n+/ni/n+ diode, J. Comput. Electron., **4**, (2005), 261–273.

[GSb05] Galler, M.; Schürrer, F.: A deterministic solver for the transport of the AlGaN/GaN 2D electron gas including hot-phonon and degeneracy effects, J. Comput. Phys., **210**, (2005), 519–534.

[Ga05] Galler, M.: Multigroup Equations for the description of the Particle Transport in Semiconductors, Series on Advances in Mathematics for Applied Sciences 70, World Scientific Publishing (2005).

[GM06] Galler, M.; Majorana, A.: Deterministic and Stochastic Simulations of Electron Transport in Semiconductors, to appear in Transport Theory and Stat. Phys.

[GS06] Galler, M.; Schürrer, F.: A direct multigroup-WENO solver for the 2D non-stationary Boltzmann-Poisson system for GaAs devices: GaAs-MESFET, J. Comput. Phys., **212**, (2006), 778–797.

[Ga90] Gamba, I.M: Behavior of the potential at the pn-Junction for a model in semiconductor theory, Appl. Math. Lett., **3**, (1990), 59–63.

[Ga93-1] Gamba, I.M: Asymptotic boundary conditions for an oxide region in a semiconductor device, Asymptotic Anal., **7**, (1993), 37–48.

[Ga93-2] Gamba, I.M: Asymptotic behavior at the boundary of a semiconductor device in two space dimensions, Ann. Mat. Pura App. (IV), **CLXIII**, (1993), 43–91.

[GP06] Gamba, I.M; Proft, J.: Local Discontinuous Galerkin schemes to linear Boltzmann equations. Analysis and simulations, preprint.

[GCG1] González, P.; Godoy, A.; Gámiz, F.; Carrillo, J.A.: Accurate Deterministic Numerical Simulation of p-n Junctions, Journal of Computational Electronics **3**, (2004), 235–238.

[GCG2] González, P.; Carrillo, J.A.; Gámiz, F.: Deterministic Numerical Simulation of 1d kinetic descriptions of Bipolar Electron Devices, to appear in Mathematics for Industry Springer Series.

[Gr85] Grisvard, P.: Elliptic Problems in Non-smooth Domains, Monographs and Studies in Mathematics, **24**, Pitman, London 1985.

[JS94] Jerome, J.W.; Shu, C.-W.: Energy models for one-carrier transport in semiconductor devices, IMA Volumes in Mathematics and Its Applications, **59**, (1994), 185–207.

[JS96] Jiang, G.; Shu, C.-W.: Efficient implementation of weighted ENO schemes, J. Comput. Phys., **126**, (1996), 202–228.

[JPMRB06] Jungemann, C.; Pham, A.; Meinerzhagen, B.; Ringhofer, C.; Boellhofer, M.: Stable discretization of the Boltzmann equation based on spherical harmonics, box integration and a maximum entropy dissipation principle, preprint 2006.

[L00] Lundstrom, M.: Fundamentals of Carrier Transport, Cambridge University Press, Cambridge 2000.

[MMM04] Majorana, A.; Milazzo, C.; Muscato, O.: Charge transport in 1D silicon devices via Monte Carlo simulation and Boltzmann-Poisson solver, COMPEL, **23**, (2004), 410–425.

[MP01] Majorana, A.; Pidatella, R.M.: A finite difference scheme solving the Boltzmann-Poisson system for semiconductor devices, J. Comput. Phys., **174**, (2001), 649–668.

[MCM05] Mantas, J.M.; Carrillo J.A.; Majorana, A.: Parallelization of WENO-Boltzmann schemes for kinetic descriptions of 2D semiconductor devices, to appear in Mathematics for Industry Springer Series.

[MR05] Mascali, G.; Romano, V.: Simulation of Gunn oscillations with a non-parabolic hydrodynamical model based on the maximum entropy principle, Compel, **24**, (2005), 35–54.

[MRS90] Markowich, P.A.; Ringhofer, C.; Schmeiser, C.: Semiconductor Equations, Springer-Verlag, New-York 1990.

[R00] Ringhofer, C.: Space-time discretization of series expansion methods for the Boltzmann Transport equation, SIAM J. Numer. Anal., **38**, (2000), 442-465.

[R03] Ringhofer, C.: A Mixed Spectral - Difference Method for the Steady State Boltzmann - Poisson System, SIAM J. Numerical Analysis **41**, (2003), 64-89.

[Sel84] Selberherr, S.: Analysis and Simulations of Semiconductor Devices, Springer, Vienna 1984.

[Sh98] Shu, C.-W.: Essentially non-oscillatory and weighted essentially non-oscillatory schemes for hyperbolic conservation laws, Lecture Notes in Mathematics **1697**, (1998), 325–432.

[To93] Tomizawa, K.: Numerical Simulation of Submicron Semiconductor Devices, Artech House, Boston 1993.

m	electron mass	$9.1095 \cdot 10^{-31} Kg$
m_*^*	effective electron mass in Si	$0.32\, m$
m_Γ^*	effective electron mass in the Γ-valley (GaAs)	$0.067\, m$
m_L^*	effective electron mass in the L-valley (GaAs)	$0.35\, m$
ρ_0	density lattice (Si)	$2330\, Kg/m^3$
	density lattice (GaAs)	$5360\, Kg/m^3$
v_s	longitudinal sound speed (Si)	$9040\, m/s$
	longitudinal sound speed (GaAs)	$5240\, m/s$
α	non parabolicity factor in Si	$0.5\, eV^{-1}$
α_Γ	non parabolicity factor in the Γ-valley (GaAs)	$0.611\, eV^{-1}$
α_L	non parabolicity factor in the L-valley (GaAs)	$0.242\, eV^{-1}$
ϵ_r	relative dielectric constant (Si)	11.7
	relative dielectric constant (GaAs)	12.90
ϵ_∞	relative dielectric constant at optical frequency (GaAs)	10.92
ϵ_v	vacuum dielectric constant	$8.85419 \cdot 10^{-12}\, F/m$
Ξ_d	acoustic-phonon deformation potential (Si)	$9\, eV$
	acoustic-phonon deformation potential (GaAs)	$7\, eV$
$D_t K$	non-polar optical phonon deformation potential (Si)	$11.4 \cdot 10^{10}\, eV/m$
	non-polar optical phonon deformation potential (GaAs)	$10^{11}\, eV/m$
$\hbar\omega_{np}$	non-polar optical phonon energy (Si)	$0.063\, eV$
	non-polar optical phonon energy (GaAs)	$0.032\, eV$
$\hbar\omega_p$	polar optical phonon energy (GaAs)	$0.032\, eV$
$\varepsilon_{0\Gamma}$	Γ-valley bottom energy (GaAs)	$0\, eV$
ε_{0L}	L-valley bottom energy (GaAs)	$0.32\, eV$
$Z_{\Gamma L}$	degeneracy from Γ to L valleys (GaAs)	4
$Z_{L\Gamma}$	degeneracy form L to Γ valley (GaAs)	1
Z_{LL}	degeneracy from L to L valleys (GaAs)	3
n_i	intrinsic concentration (GaAs)	$1.79 \cdot 10^6\, cm^{-3}$
N_I	impurity concentration (GaAs)	$10^{14}\, cm^{-3}$
$Z\mathfrak{e} = \mathfrak{e}$	elementary charge	$1.6021 \cdot 10^{-19} C$

Table 1. Parameters for Si and GaAs.